Change Detection for Monostatic Pursuit SAR GMTI—Theories and Experimental Results

Thomas K. Sjögren, *Member, IEEE*, Viet T. Vu, *Senior Member, IEEE*, Mats I. Pettersson, *Senior Member, IEEE*, and A. Gustavsson

***Abstract*— Monostatic pursuit refers to the operating mode formed by two monostatic synthetic aperture radar (SAR) systems that follow an identical orbit with a separation in a time of several seconds. The detected changes between SAR scenes with several seconds of time difference are most likely the changes caused by ground moving targets. Hence, this operating mode opens an opportunity to detect ground moving targets by SAR change detection methods. This article investigates this possibility to detect ground moving targets using change detection and to combine change detection and ground moving target indication (GMTI) for GMTI. In this combination, a GMTI method will help to classify the detected changes obtained with a change detection method. Some GMTI results are provided in the article based on the measurements in the monostatic pursuit mode with deployed targets, conducted by TerraSAR-X and TanDEM-X in Sweden in early 2015.**

***Index Terms*— Change detection, ground moving target indication (GMTI), pursuit mode, synthetic aperture radar (SAR).**

I. Introduction

GROUND moving target indication (GMTI) is an important application of synthetic aperture radar (SAR) for both military purposes, e.g., surveillance and reconnaissance, and civilian purposes, e.g., traffic monitoring. A comprehensive GMTI method is desired to include capabilities of detecting moving targets in a ground scene of interest, estimating motion parameters of detected targets, and providing images of detected targets. One of the fundamentals used for developing GMTI methods is the Doppler frequency shift caused by motions. The movement of a target in a ground scene produces Doppler frequency and if the speed of the target is high enough, it is distinguishable from the surrounding stationary clutter. The optimal schemes based on Doppler frequency and Doppler rate using the maximum likelihood criterion were developed in the early 1990s [1]. Another effect that can be used to develop GMTI methods is shadowing caused by the displacement of moving targets in SAR images. This displacement leads to the nulls in images associated with the original positions of moving targets [2]. Under the condition of strong ground backscattering, GMTI methods based on the shadowing effect can give good GMTI results. Besides the displacement, moving targets get smeared in SAR images [3]. On one hand, this effect can make GMTI more difficult. On the other hand, this effect can also be used to develop SAR GMTI methods under the principle that moving targets get refocused whereas clutter is smeared simultaneously when the SAR image formation process is carried out by the true target normalized relative speed. It is obvious that displacement and smearing are effects related only to the magnitude of SAR images. Another target feature that can be used to develop SAR GMTI methods is the phase of SAR images. The method proposed in [4] is based on the fact that the phase error in SAR images is caused by ground moving targets. The error is estimated over a SAR image and compared with a detection threshold to conclude whether a target is present or not.

Change detection is another important application of SAR. SAR change detection enables detecting changes in a ground scene between two measurements at different times. The changes can be the result of natural disasters or human legal and illegal activities. The SAR change detection methods developed are very diverse thanks to the theories such as Neyman–Pearson lemma and Bayes' theorem that can be used for method development. Different probability distributions for random variables such as complex normal distribution and bivariate gamma distribution are available to model the distribution of clutter and noise present in SAR images [5], [6]. Different processing schemes also contribute to the diversity of the change detection methods. If these methods can be used for SAR GMTI, then a large number of new SAR GMTI methods may emerge.

During the time period of October 2014 to February 2015, TerraSAR-X [7] and TanDEM-X [8] have been operating in the monostatic pursuit mode [9]. This operating mode requires TerraSAR-X and TanDEM-X satellites flying with an identical orbit in space and separated few seconds in time. With the short separation in time between the measurements, the changes in a ground scene come mainly from ground moving targets. This opens a new opportunity to detect ground moving targets not only with the available SAR GMTI methods but also with the available SAR change detection methods. In order to investigate and evaluate this new opportunity, the measurements with deployed targets were conducted around Mantorp, west of Linköping, Sweden, in 2015 using the

Manuscript received 23 May 2022; revised 17 August 2022; accepted 1 September 2022. Date of publication 16 September 2022; date of current version 7 October 2022. *(Corresponding author: Viet T. Vu.)*

Thomas K. Sjögren and A. Gustavsson are with the Swedish Defense Research Agency, 58330 Linköping, Sweden (e-mail: thomas.sjogren@foi.se; anders.gustavsson@foi.se).

Viet T. Vu and Mats I. Pettersson are with the Blekinge Institute of Technology, 37179 Karlskrona, Sweden (e-mail: viet.thuy.vu@bth.se; mats.pettersson@bth.se).

Digital Object Identifier 10.1109/TGRS.2022.3206867

TerraSAR-X and TanDEM-X satellites. The systems were configured to operate in monostatic pursuit mode with separation along-track. The separated distance corresponds to about a 10 s delay. In the ground scene, some ground moving targets with different velocities were deployed. The time for the measurements was selected at 6:30 am local time on a Saturday morning for better controlling the measurements. At the measurement time, there was almost no traffic. This allowed the vehicles to be deployed as desired and able to drive at low speeds without disturbing other vehicles. The outcome of the measurements is a dataset (SAR images) that can be used for investigating and evaluating the possibility to detect ground moving targets with the available SAR change detection methods.

In this article, we present an investigation on the possibility to use SAR change detection methods for GMTI with the data measured by two SAR systems operating in monostatic pursuit mode. It is desired that SAR change detection can provide at least the changes possibly caused by ground moving targets that can be used to indicate the presence of targets. A combination of SAR change detection and SAR GMTI for a broader context of GMTI is also addressed.

The rest of this article is organized as follows. Section II discusses about GMTI, the signature of ground moving target in a SAR image, focusing approach and local GMTI by focusing. Section III presents the change detection method that will be used for GMTI in this study. Section IV reports the setups and the data acquisition for the monostatic pursuit mode measurements that were conducted in Sweden in 2015. The experimental results and evaluations are provided in Section V. Section VI includes the concluding remarks.

II. Ground Moving Target Indication

GMTI aims at detecting moving targets in the ground scene, estimating parameters of the detected moving targets such as speed and direction of movement, and retrieving focused images of the detected ground moving targets. The presence of ground moving targets in a SAR scene leads to some effects in the SAR image that can be used as bases to develop GMTI methods for strongly reflected targets. A typical effect is smearing that can be observed easier in comparison to other effects such as shadowing. A GMTI method developed on this phenomenon is named moving target detection by focusing.

A. Ground Moving Target Signature

As shown in [10], the mathematical expression of a ground moving target signature in a SAR image formed in a slant-range plane (x, y) is given by

$$\frac{(x-x_0)^2}{\gamma^{-2}\left(\gamma^2-1\right)y_0^2}+\frac{(y-y_0)^2}{y_0^2}=1 \tag{1}$$

where (x, y) is the SAR image coordinate and γ is the normalized relative speed. It is calculated by

$$\gamma=\sqrt{1-2\left(\frac{v_g}{v_{\text{av}}}\right)\cos\Delta\phi+\left(\frac{v_g}{v_{\text{av}}}\right)^2} \tag{2}$$

where v_g and v_{av} are the speeds of the ground moving target and the SAR platform, respectively, $\Delta\phi$ is the angle formed by the target velocity and the platform velocity. Equation (1) is the function of either an elliptic curve or a hyperbolic curve centered at (x_0, y_0). This center relates to the true position of the moving target (x_g, y_g) by

$$x_0=x_g-\frac{v_g\sin\Delta\phi}{v_{\text{av}}-v_g\cos\Delta\phi}y_g \tag{3}$$

and

$$y_0=y_g\sqrt{1+\left(\frac{v_g\sin\Delta\phi}{v_{\text{av}}-v_g\cos\Delta\phi}\right)^2}. \tag{4}$$

By setting $\cos\alpha=1$, the limit of γ is given by

$$1-\frac{v_g}{v_{\text{av}}}\le\gamma\le1+\frac{v_g}{v_{\text{av}}}. \tag{5}$$

In the general case, for $\gamma>1$, i.e., $\gamma^2-1>0$, (1) will be a function of ellipse. Since $(\gamma^2-1)/\gamma^2<1$, the major axis lies in y-axis while the minor axis corresponds to x-axis. The axial ratio of the ellipse (1) is determined by

$$\text{AR}=\frac{\gamma}{\sqrt{|\gamma^2-1|}} \tag{6}$$

and the tilt angle is $\tau=\pi/2$. In the opposite case $\gamma<1$, i.e., $\gamma^2-1<0$, (1) represents a function of hyperbola. Since $(\gamma^2-1)/\gamma^2<0$, the major axis lies in y-axis or the tilt angle is $\tau=\pi/2$. The axial ratio of the hyperbola is also given by (6).

For space-borne SAR systems like TanDEM-X and TerraSAR-X [6], [7], the orbits are circular. The speed of the SAR platform is converted to the ground speed. Herein, v_{av} refers to this ground speed. It is usually extremely high in comparison to speeds of any ground moving target $v_g\ll v_{\text{av}}$. The normalized relative speed given by (2) can be approximated by $\gamma\approx1$. In this case, the minor axis of the ellipse approaches zero and, as consequence, the axial ratio approaches infinity (AR $\approx\infty$). Equation (1) is approximated by a function of a line going through the center (x_0, y_0). The signature of a ground moving target in a SAR image in this special case is a line that is parallel to the SAR platform's orbit. The displacement is only in the azimuth direction because of the approximation in this case $y_0\approx y_g$.

B. Locally Focusing of Ground Moving Target

The locally focusing technique for ground moving target was derived from the Range Migration algorithm in [11]. According to the Range Migration algorithm [12], a SAR image of a ground scene $\Im(x, y, t=-t_0)$ can be expressed in the form of a 2-D inverse Fourier transform by

$$\begin{aligned}\Im(x,y,t=-t_0)&=\frac{1}{(2\pi)^2}\iint S\left(k_x,y=0,\frac{c}{2}\sqrt{k_x^2+k_y^2}\right)\\&\quad\times\exp\left\{-jt_0(c/2)\sqrt{k_x^2+k_y^2}\right\}\\&\quad\times\frac{c}{2}\exp\left\{j\left(k_xx+k_yy\right)\right\}\frac{k_y}{\sqrt{k_x^2+k_y^2}}dk_xdk_y\end{aligned} \tag{7}$$

where t_0 is the time from transmission of signal until the data recording starts, $S(k_x, y = 0, (c/2)(k_x^2 + k_y^2)^{1/2})$ denotes the 2-D Fourier transform of data after the Stolt interpolation, k_x and k_y are the azimuth and range wave numbers, respectively. The azimuth wavenumber is defined by

$$k_x = \frac{2\pi f_x}{v_{\text{av}}} \tag{8}$$

where f_x denotes azimuth frequency and lies in the range [−pulse repetition frequency (PRF)/2, +PRF/2]. The wavenumbers and the radar angular frequency ω are linked together by the relationship

$$\omega = \frac{c}{2}\sqrt{k_x^2 + k_y^2} \tag{9}$$

and (9) is the base for the Stolt interpolation.

Assume that a moving target is present in the ground scene and the normalized relative speed is determined by γ. The moving target will be displaced and smeared in the SAR image (7) in a form of an elliptical or hyperbolic curve in the SAR image of the ground scene. To refocus it on a new SAR image, this new SAR image should have the following expression:

$$\begin{aligned}\tilde{\Im}(x, y, t = -t_0) &= \frac{1}{(2\pi)^2}\iint \tilde{S}\left(k_x/\gamma, y = 0, \frac{c}{2}\sqrt{(k_x/\gamma)^2 + k_y^2}\right) \\ &\quad \times \exp\left\{-jt_0(c/2)\sqrt{(k_x/\gamma)^2 + k_y^2}\right\} \\ &\quad \times \frac{c}{2}\exp\left\{j\left(\frac{k_x x}{\gamma} + k_y y\right)\right\}\frac{k_y}{\sqrt{(k_x/\gamma)^2 + k_y^2}}\frac{dk_x}{\gamma}dk_y\end{aligned} \tag{10}$$

that is (10) in [11]. The term k_x/γ in (10) replacing k_x in (7) is interpreted by that the speed of the platform is rescaled with the normalized relative speed γ. Equation (10) implies that to refocus the moving target, an extra interpolation is required

$$\begin{aligned}&S\left(k_x, y = 0, \frac{c}{2}\sqrt{k_x^2 + k_y^2}\right) \\ &\qquad \longmapsto \tilde{S}\left(\frac{k_x}{\gamma}, y = 0, \frac{c}{2}\sqrt{\left(\frac{k_x}{\gamma}\right)^2 + \tilde{k}_y^2}\right)\end{aligned} \tag{11}$$

where $\tilde{k}_y$ fulfills the condition

$$\omega = \frac{c}{2}\sqrt{\left(\frac{k_x}{\gamma}\right)^2 + \tilde{k}_y^2}. \tag{12}$$

The relationship between k_y and $\tilde{k}_y$ can be easily shown to be

$$k_y = \sqrt{\left(\frac{1}{\gamma^2} - 1\right)k_x^2 + \tilde{k}_y^2}. \tag{13}$$

Refocusing a moving target in the new image of a ground scene also means that the clutter will be smeared in it.

C. Local GMTI

The processing scheme for local GMTI is summarized as follows [11].

1) Selecting area of interest.
2) Testing different hypotheses on γ for (10).
3) Retrieving highest magnitudes for each hypothesis.
4) Locating peak(s).
5) Minimizing false alarms.

An area of interest is not necessarily the area where a moving target is present in the ground scene. It is the SAR image area, where the target is displaced into it due to the movement and appears as an elliptic or hyperbolic curve. The calculation on this displacement is based on (3) and (4).

The range of hypotheses can be derived from (2) by setting $\cos\alpha = \pm 1$ and providing the maximum expected ground moving target speed, v_g, for selected target types. For example, if the maximum speed of targets is 10% speed of the SAR platform, a range of hypotheses will be given by $\gamma \in [0.9\ 1.1]$. The step size between hypotheses on normalized relative speed must also be taken into account since it affects the detection time of the method. An optimum quantization step size $\Delta\gamma$ between hypotheses is suggested in [13] as a function of minimum range, center frequency, aperture length, the maximum loss of intensity and the so-called detection constant. Besides the regular step size, numerical methods such as the midpoint method can be used to have an irregular step size in order to minimize the detection time.

For a small area of interest and under the assumption that there is no more than one ground moving target displaced into it, the graph representing the relationship between normalized relative speed and magnitude has only one peak. This peak corresponds to the case that the moving target is refocused with a correct normalized relative speed. We can also select a large area of interest with more than one displaced target. Several peaks retrieved from the graph need to be examined before concluding how many targets are displaced into the area of interest.

To minimize the false alarms, morphological operations such as erosion and dilation should be applied. This allows for those detections with dimension below the spatial resolutions of the SAR system will be considered to be false alarms, whereas the detections separated less than the spatial resolutions of the SAR system will be merged. In the case where a selected structuring element for the morphological operations is larger than the spatial resolutions, the morphological operations can remove true ground moving targets. Therefore, a selection of structuring elements should be based on moving target backscattering and the parameters such as speed and direction.

III. Change Detection

A large number of change detection methods have emerged though time. A common processing sequence for change detection usually includes: SAR image formation, detection, and false alarm minimization. The detection step requires two images: one is defined as a reference image and the other is defined as surveillance (updated) image. The data to form

the reference image and surveillance one is measured for the same SAR scene but at different time periods. In an ideal case, the changes in the ground scene can be detected by subtraction or logarithmic division of the reference image to the surveillance image, followed by thresholding. However, the presence of clutter and noise in the SAR images prevents subtraction or division and thresholding from providing reliable change detection results. In practice, change detection methods usually require much more complex operations to obtain them. In this study, a change detection method derived with Neyman–Pearson lemma is considered, in which simplicity and efficiency are the motivations for the choice.

The Neyman–Pearson lemma has been used to derive statistical hypothesis tests for SAR change detection [6], [14], [15]. It is good to highlight that certain assumptions on targets must be made to calculate these statistical hypothesis tests [16] and such assumptions affect change detection results significantly. A recent publication proposed a way to avoid unwanted assumptions by reformulating the likelihood ratio test in the following form [17]:

$$\frac{P(\mathbf{u})}{P(\mathbf{u}|H_0)} \lessgtr \lambda \tag{14}$$

where $P(\mathbf{u}|H_0)$ is the probability of variable $\mathbf{u}$, $P(\mathbf{u}|H_0)$ is the probability of variable $\mathbf{u}$ given H_0, and λ is the threshold.

In the SAR change detection context, the variable $\mathbf{u}$ can be either scalar or vector that contains information about reference and surveillance images. Since the processing time plays an important role in GMTI, the dimension of the variable $\mathbf{u}$ should be minimum, i.e., $\mathbf{u}$ should be a scalar instead of a vector. The hypothesis H_0 corresponds to a statement of no change, whereas the hypothesis about the change is denoted by H_1. Without change, the variable $\mathbf{u}$ is assumed to contain only clutter and noise

$$H_0 : \ \mathbf{u} = \mathbf{c} + \mathbf{n}. \tag{15}$$

If we denote the change by the variable $\mathbf{s}$, the hypothesis H_1 is defined by

$$H_1 : \ \mathbf{u} = \mathbf{s} + \mathbf{c} + \mathbf{n}. \tag{16}$$

A. Scalar Data Formation

As mentioned, the variable $\mathbf{u}$ for SAR change detection is a scalar and should contain information about reference and surveillance images. For the reference and surveillance images acquired on two different dates and/or with two different SAR systems, system calibrations are necessary. Assume that the SAR systems are calibrated. We also assume that the reference and surveillance images are perfectly coregistered. To create this variable, we first remove the phase information from the complex surveillance image and the reference image. The remains in the images are only magnitudes. Then we subtract the surveillance image from the reference image to get the unique difference image that is represented in a matrix like the surveillance image and the reference image. The variable $\mathbf{u}$ is one sample of the difference image or in other words, an element of the data matrix. This process is expressed by

$$\mathbf{u} = \Im(m, n) = |\Im_u(m, n)| - |\Im_r(m, n)| \tag{17}$$

where the subscripts $_r$ and $_u$ denote reference and surveillance (updated), respectively.

B. Statistical Hypothesis Test

An appropriate model for clutter and noise present in $\Im$ can be used for calculating $P(\mathbf{u}|H_0)$. An investigation into the statistics of $\Im$ is therefore necessary. Under the assumption that the clutter and noise present in $\Im$ is normally distributed, the probability $P(\mathbf{u}|H_0)$ is calculated from the probability density function

$$\rho(\mathbf{u}|H_0) = \frac{1}{\sigma\sqrt{2\pi}} \exp\left(-\frac{1}{2}\left(\frac{\mathbf{u}-\mu}{\sigma}\right)^2\right) \tag{18}$$

where μ and σ are mean and standard deviation, respectively, that can be estimated from $\Im$ using the maximum likelihood approach or the local frequency ratio approach. However, the local frequency method allows the effective estimation of parameters with less information. In addition, the method can provide locally accurate estimations.

The probability $P(\mathbf{u})$ can be calculated directly from the data histogram of $\mathbf{u}$. To create the data histogram, we arrange $\Im$ into bins. Assuming that the value of $\mathbf{u}$ belongs to a certain bin, $P(\mathbf{u})$ will be the ratio of the frequency with respect to that bin to the sum of the frequencies given by all bins.

Armed with $P(\mathbf{u}|H_0)$ and $P(\mathbf{u})$, we can easily conduct the likelihood ratio test using (14).

C. Change Detection

The processing scheme for change detection is summarized as follows.

1) Performing calibration and coregistration for surveillance and reference images.
2) Selecting area of interest.
3) Forming difference image using (17).
4) Estimating parameters for probability density function and forming data histogram.
5) Calculating statistical hypothesis test for each image sample using (14).
6) Thresholding.
7) Minimizing false alarms.

The first and the last processing steps of the change detection scheme are identical to that of the local SAR GMTI. It is worth mentioning that after calculating the statistical hypothesis test for each image sample, we get a matrix of ratios. Hence, the values of this matrix vary in a very wide range $(1, \infty)$. The value 1 corresponds to the case where $P(\mathbf{u}) = P(\mathbf{u}|H_0)$. This corresponds to the ideal case where there is no change and the distribution of $\Im$ is perfectly matched with the model for clutter and noise. The ratio approaches infinity when $P(\mathbf{u}|H_0)$ approaches 0. This corresponds to the case where a change is present and $\mathbf{u}$ is beyond the values covered by the model for clutter and noise. In the linear scale, the separation between the values of the matrix can be very large. A conversion from a linear scale to a logarithmic scale is therefore applied to the matrix of ratios before thresholding,

resulting into

$$\log\left[\frac{P(\mathbf{u})}{P(\mathbf{u}|H_0)}\right] \lessgtr \log(\lambda). \tag{19}$$

In theory, if the data histogram part containing only clutter and noise is totally matched with the probability density function, the threshold should be about $\lambda = 1$ or $\log(\lambda) = 0$. In practice, there is always a mismatch between them. The threshold should therefore be set by $\log(\lambda) > 0$.

IV. Change Detection for GMTI

The monostatic pursuit mode requires two identical monostatic SAR systems. One system measures the ground scene of interest at a certain time instant and after a few seconds, another system performs the same measurement using the same orbit. Two SAR images, a reference and surveillance, are formed from the measured data and then coregistered. With the short separation in time between the measurements, the ground scene is considered to be unchanged except ground moving targets. The clutter caused by the large objects and trees should be stable. There might be changes caused by, for instance, the tree branches but these changes are supposed to be small in comparison to the changes caused by the ground moving targets. The targets migrate through many resolution cells during the time separation between measurements. For the short measurement time and the short separation time, the ground moving targets are likely still within the scene. Under these circumstances, it is possible to detect ground moving targets not only by GMTI methods but also by change detection methods. It is also possible to detect the slow-moving targets or even targets changing status from standing to moving between the measurements. The initial investigation on change detection for GMTI can be found in [18].

A. GMTI and Change Detection

Assume that there is a ground moving target present in the ground scene during the first measurement performed by a SAR system. After the image formation process, the target is smeared as a curve and the center of the curve is displaced to a coordinate (x_1, y_1) in the SAR image.

After a few seconds (Δt), the second measurement is performed by another SAR system. The target is assumed to be still present in the SAR scene and move with the same velocity. In the image formed with the second measurement data, the target is defocused with the same form and the center of the curve is now displaced to coordinates (x_2, y_2).

If the image formed with the first measurement data is assigned the role of the reference image and the other is assigned the role of the surveillance image, a change centered at (x_2, y_2) will be detected under the assumption that the change detection method presented in Section III works well and detects correctly the change. If we exchange the roles of reference and surveillance images and apply the same change detection method, under the same assumption, a change centered at (x_1, y_1) will be detected. The change detection results show that

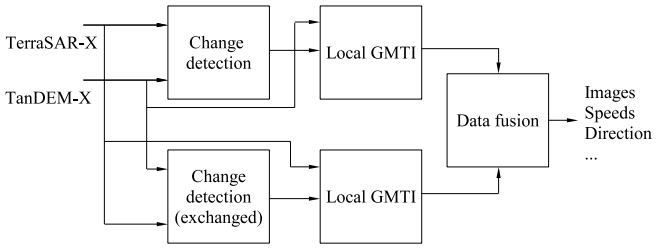

Fig. 1. General processing scheme for SAR GMTI using change detection.

1) There is a ground moving target displaced to the area of interest.
2) The signature of the detected target change from the coordinates (x_1, y_1) to the new coordinates (x_2, y_2) over the time Δt.

Having obtained estimates of moving distance and moving time, estimating the speed, the direction and the relative speed of the detected target from the coordinates is straightforward. The true target trajectory can also be retrieved using (3) and (4). The estimated relative speed allows retrieving the image of the detected target using the focusing approach presented in Section II.

Hence, SAR GMTI using a change method can have capabilities such as detecting moving targets in a ground scene of interest, estimating motion parameters of detected targets, and locating the trajectories of detected targets.

B. Processing Schemes for SAR GMTI Using Change Detection

Fig. 1 presents a general processing scheme for SAR GMTI using change detection with two change detection blocks, two GMTI blocks and a data fusion block. In the general case, a change detection method detects only the changes occurring on the surveillance image under the assumption that there is no change on the reference image. The typical examples are the change detection methods proposed in [5], [6] using the likelihood ratio test and bivariate probability distributions to model clutter and noise. For SAR GMTI using change detection, the changes caused by moving targets also appear on the reference images and detecting these changes is important for GMTI. This explains why there are two change detection blocks in the processing scheme and the roles of reference and surveillance are exchanged in the blocks.

In a less general case, where the surveillance and reference images are combined with subtraction or logarithmic division and the clutter and noise model can be represented by a symmetrical probability distribution density function, a single change detection block is required. The positive changes (the targets appear in the surveillance image) and the negative changes (the targets appear in the reference image) can be detected by thresholding the right tail and the left tail of the probability distribution density function. Fig. 2 presents the detailed processing scheme with one change detection block, showing a combination of the change detection method presented in Section III and the local GMTI method presented in Section II. The aim of this combination is to obtain not

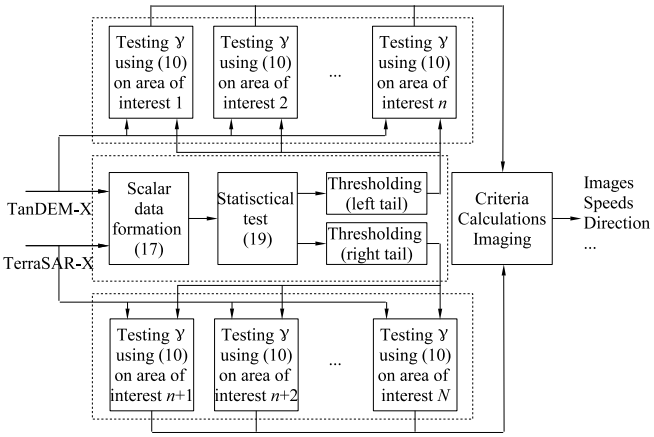

Fig. 2. Processing scheme for the proposed method.

only the desired capabilities of GMTI as mentioned but also more reliable GMTI results in comparison to the GMTI results obtained by only a change detection method or only the local GMTI method.

Among the processing steps for change detection, thresholding, and minimizing false alarms should be performed for the GMTI purpose. A low threshold for change detection should be selected, e.g., $\lambda = 1$ or $\log(\lambda) = 0$. This low threshold ensures that all changes, even very small changes, are not ignored by the change detection method. The morphological operations should be designed so that only the detected changes with the signature (1) are considered, whereas the detected changes without this signature are eliminated. The dilation is therefore first applied to the detected changes. The adjacent detected changes will be merged together if the separation between them is below the spatial resolutions of the SAR system. The erosion is then applied to the detected changes and the changes are merged by the dilation. The structuring element for the erosion should be matched with the ground moving target signature (a line). The detected changes and the changes merged by the dilation, that do not match with the structuring element, will be considered false alarms and removed from the change detection results. In theory, we may find the centers of the detected changes (x_1, y_1) and (x_2, y_2) and then estimate speed, the direction and the relative speed of the detected targets. In practice, finding the relations between the detected changes is not easy when there are several targets displaced to the area of interest for change detection. In addition, it is also difficult to determine the centers of the detected changes. For this reason, the next processing step will be the local GMTI.

The local SAR GMTI method presented in Section II is applied to the two images. The change detection results help to locate the areas of interest for GMTI. They need only cover the detections with ground moving target signature and their surroundings. For small areas of interest, the processing time for testing the hypotheses will be very short. The peak of the graph representing the relationship between normalized relative speed and magnitude corresponds to the case a moving target is focused with a correct normalized relative speed. After this processing step, the information about possible detected moving targets and their normalized relative speeds are available for two images.

For concluding which detections are moving targets and which detections are not, a data fusion step is necessary for the processing scheme for SAR GMTI (Fig. 1). The following criteria can be used for data fusion.

1) A moving target should be detected by both change detection blocks.
2) Two detections of a moving target should be close together and the separation is limited by the maximum speed of targets.
3) Two detections of a moving target should have the same normalized relative speeds γ.

The detections that meet these criteria will be classified as ground moving targets, whereas other detections will be classified as false alarms.

With the retrieved γ, we can form the images of the detected moving targets. For the detected moving targets that are refocused in the SAR images, we can easily locate (x_1, y_1) and (x_2, y_2) and then estimate speeds and the directions of those targets.

V. Monostatic Pursuit Mode Measurements

The measurements were performed in February 2015 with the aim to investigate the possibilities to use change detection for the monostatic pursuit SAR GMTI and to combine GMTI methods and change detection. The arrangements are depicted in Fig. 3. The given time for the measurements was about 6:30 am on a Saturday.

A. TerraSAR-X and TanDEM-X

TerraSAR-X, an X-band SAR sensor, was launched in 2007 [7]. The system operates in three different modes: staring spotlight, stripmap, and scanSAR modes, providing a wide range of products from high-resolution images to images covering large ground scenes. The system can be configured for various polarizations such as single [horizontal linear transmission and horizontal linear reception (HH) or vertical linear transmission and vertical linear reception (VV)], dual [HH/VV, HH/horizontal linear transmission and vertical linear reception (HV), or VV/vertical linear transmission and horizontal linear reception (VH)], and even quadrature (VV, HV for one channel and VH, HH for the other) [19]. The applications based on TerraSAR-X include 2-D and 3-D topographic mapping, surface movement monitoring, change detection, defense, and security applications, etc.

TanDEM-X is almost identical to TerraSAR-X, and when operating in cooperation with TerraSAR-X, they create a SAR interferometer [8]. TanDEM-X was launched in 2010. It was developed for the purpose of generating a global digital elevation model (DEM) and to demonstrate new radar imaging techniques and applications. TanDEM-X and TerraSAR-X have been flying in close formation, down to under a hundred meters apart, with adjustable baselines in across- and along-track directions when generating the DEM. The difference in incidence angle to the scene between the two platforms is the basis to determine the interferometric height. TerraSAR-X and TanDEM-X formation also offers flexibility in sharing operational functions for both the TerraSAR-X and TanDEM-X mission. The pursuit monostatic mode for

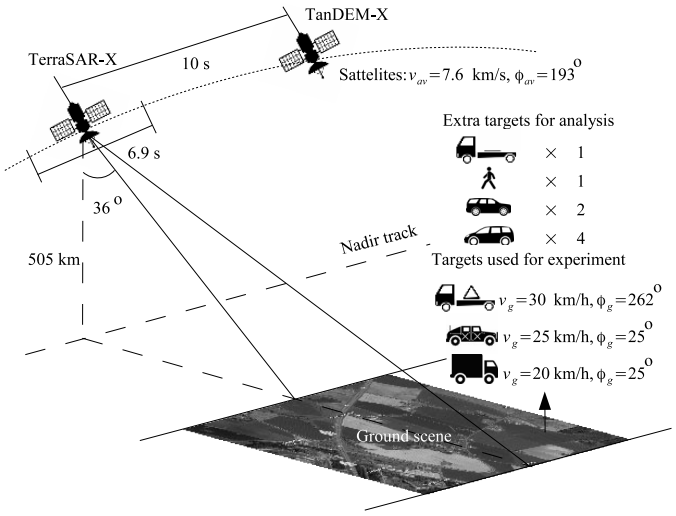

Fig. 3. Arrangements of monostatic pursuit mode measurements.

GMTI was demonstrated for TerraSAR-X/TanDEM-X. As the background to this pursuit of monostatic mode, airborne GMTI has been extensively studied for many years, and several algorithms have been developed [20], [21].

TerraSAR-X and TanDEM-X have been operating in the pursuit monostatic mode only a few time periods, the first one was during the commissioning phase in 2010 and the second was from the end of 2014 until the beginning of 2015 as the first part in the science phase of the TanDEM-X mission. The pursuit monostatic mode [9] requires TerraSAR-X and TanDEM-X to fly in an identical satellite orbit in space and separated few seconds in time. During the commissioning phase this time separation was about 2.5 s and in the science phase it was 10 s. The selection of a suitable value for the delay in seconds for GMTI was analyzed in [22], in which it is found that the time separation between the satellites should be between 2 and 4 s. The reason the separation should not be larger is due to the expected acceleration for passenger cars.

During the measurements, TerraSAR-X and TanDEM-X were arranged in the pursuit monostatic mode as depicted in Fig. 3. The orbits of the satellites TerraSAR-X and TanDEM-X were identical but TanDEM-X is behind TerraSAR-X with a separation along-track. For these specific measurements, the distance corresponded to a 10 s delay in time. The measurements were in descending pass with the incidence angle of about 36°. The primary parameters of TerraSAR-X and TanDEM-X for the measurements are summarized in Table I.

Since high-resolution images for the investigation are of interest, both satellite systems were operating in the staring spotlight imaging mode [23]. For this mode, the azimuth resolution is about 0.230 m while the slant range resolution is about 0.588 m. The pixel spacings are 0.166 m in azimuth and 0.455 m in slant range. The coverage area is 3000 m in azimuth times 3600 m in range. Both satellites were operating using HH polarization. Fig. 4 shows the image of the SAR scene.

B. Ground Scene and Deployment

The selected test site for the measurements is Mantorp, a small village outside the town of Linköping, Sweden.

TABLE I
PARAMETERS OF TERRASAR-X AND TANDEM-X FOR GMTI EXPERIMENT

Parameter	TerraSAR-X&TanDEM-X
Platform speed v_{av}	7.6 km/s
Platform altitude h	505 km
Incidence angle θ	36°
Center frequency f_c	9.65 GHz
Bandwidth B	300 MHz
Pulse repetition frequency (PRF)	4448 Hz
Integration time t_i	6.9 s
Minimum range $y_{\min}$	624 km
Satellite movement direction ϕ_{av}	193°

The reasons for this selection include easy deployment, availability of smaller roads, and a highway in the favorable geometry regarding the satellite orbits. Furthermore, the area mainly consists of farmland, minimizing the risk of interference from forest clutter and houses. This means fewer false alarms in the vicinity of targets and a low probability of targets being obscured. Since the time for the measurements was about 6:30 am on a Saturday morning, there was almost no traffic. This allowed the vehicles to be deployed as desired and able to drive at low speeds without disturbing other vehicles. The test site was also well suited due to the variety of movement directions. However, there was snow on the ground during the measurements and the temperature was below 0°.

At the time of measurement, the target deployment included several ground vehicles. Among deployed targets, one of the targets, a truck, was selected to have a reflector mounted on the top. This ensured that there would be a clear strong controlled signal in the image. This reflector was mounted and directed as similar as possible with two deployed reflectors in the ground scene. This target will be used mainly for an illustration of the GMTI using the change detection method presented in Section IV. Other deployed targets, e.g., a moving truck and a military vehicle, are also used to show the practical issues of the proposed method. For the deployed targets, the positions were logged with global positing system (GPS) devices. Fig. 3 provides information about the speeds and the driving directions of these targets with respect to the satellites' descending orbit.

VI. EXPERIMENTAL RESULTS

The GMTI results presented in this section are retrieved from two areas of interest marked by the white rectangles in Fig. 4. The area of interest is selected according to the true locations of the vehicles and the possible displacements. We consider here the area of interest marked by the solid-line rectangle. The road in the lower right was an arterial where the truck with the mounted reflector on top was moving during the measurements. This area of interest will be used to illustrate the operation of the change detection for the GMTI method presented in Section IV and the block diagram given in the lower part of Fig. 1. Because the change detection is based on a hypothesis statistical test, it is necessary to investigate

Fig. 4. Image of ground scene (Mantorp, west of Linköping, Sweden) generated by the SAR data acquired in February 2015 by TerraSAR-X. Acquisition mode is staring spotlight with HH polarization. The transmission bandwidth is 300 MHz and the center frequency is 9.65 GHz. The azimuth and range resolutions are about 0.230 and 0.588 m, respectively. White rectangles mark areas of interest where GMTI using change detection is tested.

the statistic of the considered data (parts of difference image covering the areas of interest).

A. Statistic of Data

Two coregistered SAR images obtained from the measurements are placed at the inputs of the change detection block in the block diagram given in the lower part of Fig. 1. Assume that the TerraSAR-X image is assigned the role of reference, i.e., $\Im_r$, and the TanDEM-X one is assigned the role of surveillance, i.e., $\Im_u$. The difference image is formed using (17) and presented by a matrix. The area of interest marked with a solid-line rectangle is extracted from the difference image to investigate the statistic. It includes several types of ground covers, e.g., buildings, houses, forests, fields, and roads. The data histogram of the area of interest is provided in Fig. 5. The probability density function of a normal distribution (18) is plotted in the same figure, in which the mean μ and the standard deviation σ of the function are estimated by the local frequency ratio method. The plotted probability density function matches well with the data histogram.

In the same figure, we also plot the probability density function (18), in which the parameters μ and σ are estimated by the maximum likelihood method. We can see a significant mismatch between the data histogram and the probability density function. This significant mismatch is due to the specular reflections originating from the roofs of buildings or the ground objects randomly forming trihedral and dihedral corners. The maximum likelihood method considers all data samples, including a large number of samples associ-

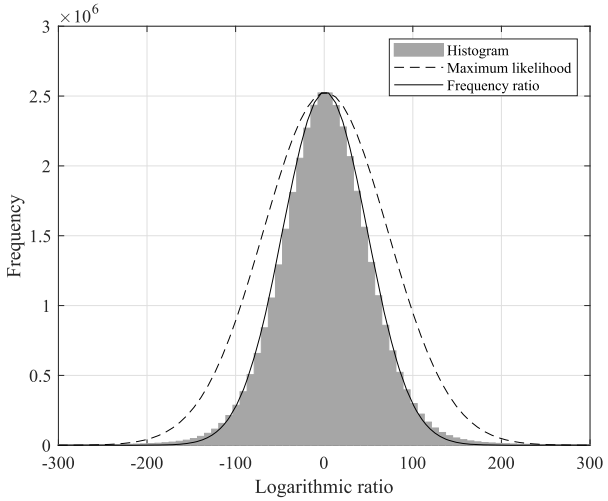

Fig. 5. Data histogram and probability density functions with parameters estimated by maximum likelihood and ratio frequency methods.

TABLE II
DEPLOYMENT OF TARGETS IN EXPERIMENT 1

Target	Type	True speed	True direction	Detection	Estimated speed	Estimated direction
Target 1	Truck with reflector	30 km/h	262°	Yes	31.2 km/h	262.8°
Target 2	Light military vehicle	20 km/h	25°	Yes	17.9 km/h	28.2°
Target 3	Moving truck	25 km/h	25°	Yes	25.0 km/h	28.2°
Target 4	Minibus	35 km/h	262°	No		
Target 5	Minivan	20 km/h	336°	No		
Target 6	Minivan	30 km/h	336°	No		
Target 7	SUV	70 km/h	75°	No		
Target 8	Person with reflector	4.5 km/h	290°	Yes	4.4 km/h	284.1°
Target 9	Truck without reflector	30 km/h	290°	Yes	29.4 km/h	284.1°
Target 10	Minibus	20 km/h	20°	Yes	15.5 km/h	20°
Target 11	SUV	20 km/h	20°	Yes	15.5 km/h	20°
Results				Probability	Error	Error
				70%	10%	3%

ated with the specular reflections, to estimate the parameters for the probability density function. For this reason, the local estimation like the ratio frequency method will give better estimations.

We can also exchange the roles of reference and surveillance. In this case, the difference image formed using (17) gives the horizontally flipped versions of the data histogram and the probability density function given in Fig. 5.

B. Change Detection

In Fig. 5, we normalize the probability density function with the peak frequency of the data histogram. With this normalization, the likelihood ratio test (14) will be given by the ratio of $f(\mathbf{u}|H_0)$ to the frequency with respect to the bin, that $\mathbf{u}$ belongs to. The samples of the difference image that results in $P(\mathbf{u}) > P(\mathbf{u}|H_0)$ due to the mismatch between the data histogram and the probability density function will be excluded from the calculation. The corresponding surveillance image pixels are assigned directly to the hypothesis H_0, concluding no change.

Calculating likelihood ratio test (14) is applied to the samples $\mathbf{u} \geq \sqrt{\sigma}$ to detect the positive changes and $\mathbf{u} \leq -\sqrt{\sigma}$ to detect the negative changes. The samples $-\sqrt{\sigma} < \mathbf{u} < \sqrt{\sigma}$ are therefore ignored and the corresponding surveillance image pixels are assigned directly to the hypothesis H_0. This helps to reduce the computation cost. The result is a matrix of likelihood ratios.

As discussed in Section III, the detection threshold is set to $\lambda = 1$. The likelihood ratios below $\lambda = 1$ will be assigned to the hypothesis H_0. The likelihood ratios above $\lambda = 1$ will be further processed with the morphological operations. We consider three morphological operations, two erosion and one dilation, for minimizing false alarms. First, we remove the detections smaller than the spatial resolutions of TerraSAR-X and TanDEM-X. Based on the spatial resolutions and the element spacings, a structuring element 2×2 (azimuth $\times$ range samples) is suitable for this erosion operator. Then, we merge the adjacent detections that are separated less than the spatial resolutions of the systems. The structuring element 2×2 pixels is used again in this dilation operator. Finally, another erosion is applied to remove the detections without the signature of ground moving target. For this erosion operator, a structuring element 12×2 (azimuth $\times$ range) is reasonable under the consideration of the smearing caused by moving targets and the dimensions of moving targets of interest. The detections with the dimensions smaller than 12×2 pixels or 2.00×0.91 m will be removed from the change detection results.

With a reference to the processing scheme given in the lower part of Fig. 1, Fig. 6(a) shows the positive changes after thresholding (right tail) with totally six detections marked by the red dots. The detection with a clear signature of ground moving target belongs to the truck with the corner reflector (Target 1 in Table II). Two detections in the upper right correspond to the power lines that were swinging due to the weather. The remaining three detections are unknown. The location of the one in the upper left corresponds to the yard of a house. The locations of the two detections in the middle correspond to the different parts of a house, in which one corresponds to the roof of the house and the other to the roof of a small storage building. It is good to highlight that the roof of the storage building is made of corrugated metal sheets combined with steel rods. A small change in incident angle can result in change detections.

The negative changes that are achieved after thresholding (left tail) with totally ten detections marked with the green dots are given in Fig. 6(b). These change detection results are equivalent to the ones when the roles of reference and

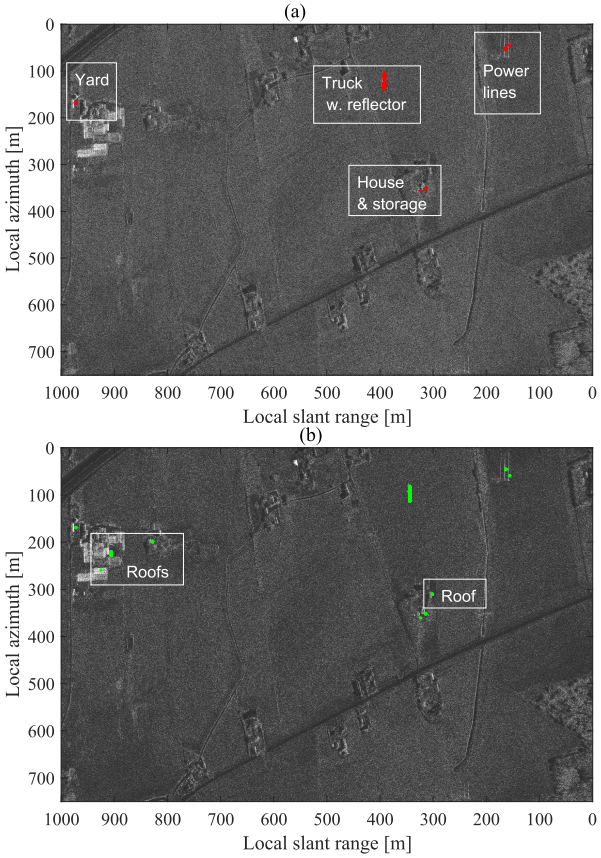

Fig. 6. Change detection results for area of interest marked by solid-line rectangle in Fig. 4. (a) Reference: TerraSAR-X, surveillance: TanDEM-X. (b) Reference: TanDEM-X, surveillance: TerraSAR-X.

surveillance are exchanged. After exchanging, the TerraSAR-X image is assigned the role of surveillance and the TanDEM-X one is assigned the role of reference.

The positive and negative changes can be analyzed as follows.

1) The detection with a clear signature of ground moving target belongs to the truck with the corner reflector. Due to the movement, the truck is detected at two different positions. This difference can be used to estimate the speed and the driving direction of the truck.
2) Two detections in the upper right correspond to the same power lines. Due to the random swinging, the power lines are detected at two different positions. We do not need to investigate these detections further for the GMTI purpose.
3) The changes in the yard of the same house in the upper left are also detected. However, the positive and negative changes belong to different parts of the same object. It can be the result of a small change of the object due to weather, but it can also be the result of imperfect coregistration. Therefore, this detection will not be further investigated for the GMTI purpose.
4) The changes in the roof of the same house and the roof of the same storage building are detected. It is most likely due to the structure of the roof (corrugated metal sheets combined with steel rods). Therefore, these detections will not be further investigated for the GMTI purpose.
5) Four remaining negative changes, that are not linked to any positive changes, belong to roofs of different houses in the SAR scene. They are classified directly as false alarms and will not be further investigated for the GMTI purpose.

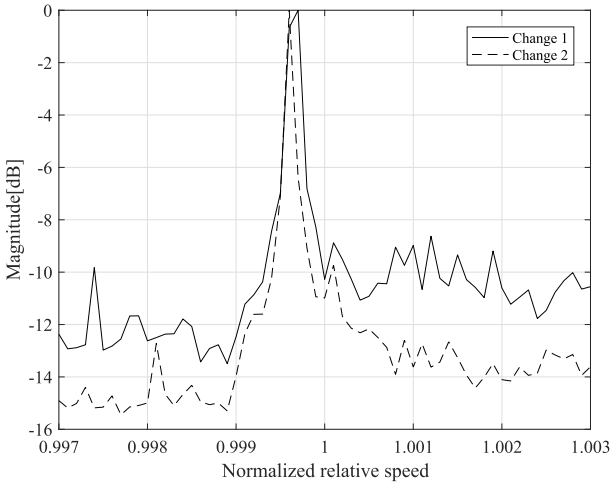

Fig. 7. Graph representing the relationship between normalized relative speed and magnitude (area of interest marked by solid-line rectangle in Fig. 4).

C. Local GMTI

The analysis of the change detection results defines the areas of interest for local GMTI. The areas of interest are very small areas as given by the red and green dots and the small areas surrounding these dots.

For the first local GMTI block using the TanDEM-X image (with the reference to the lower part of Fig. 1), there is only one area of interest corresponding to the location, where the truck with the corner reflector is displaced. It is defined by the red line (formed by the dots) and the area surrounding it. An area 41.6 $\times$ 2.73 m or 250 $\times$ 6 samples will cover the ground moving target signature.

Based on (5), the speed of the platform given in Table I, 7.6 km/s, and the maximum speed of a truck 80 km/h or 0.02 km/s, the range of normalized relative speed is estimated by $\gamma \in [0.997\ 1.003]$. A selected step size $\Delta\gamma = 1 \times 10^{-4}$ requires 61 tests. Fig. 7 plots the graph (Change 1) representing the relationship between normalized relative speed and magnitude obtained with the first local GMTI block.

The peak is found at the hypothesis $\gamma = 0.9997$, at which the detected change is best focused. This indicates that the change detected by the change detection block is most likely a ground moving target with a relative speed of $\gamma \approx 0.9997$.

For the second local GMTI block using the TerraSAR-X image, there is also one area of interest corresponding to the location, where the truck with the corner reflector is displaced after 10 s. It is defined by the green line (formed by the dots) and the area surrounding. The same parameters for the area of interest, the same range of normalized relative speed, and the same step size are used in the second local GMTI block.

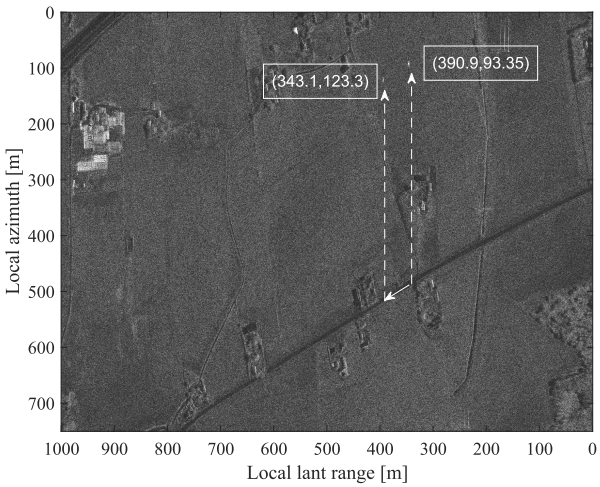

Fig. 8. Area of interest for change detection with integrated images of detections (area of interest marked by solid-line rectangle in Fig. 4).

The local GMTI result obtained with the second local GMTI block (Change 2) is reported in the same figure, Fig. 7. The result is interpreted as that the change detected by the change detection block is most likely due to a ground moving target with a normalized relative speed of $\gamma \approx 0.9996$.

D. Data Fusion

The first and second local GMTI blocks provide two detections with two different normalized relative speeds, $\gamma = 0.9997$ and $\gamma = 0.9996$. The difference between the two values is just 0.001%. These values are used to form the SAR images of the refocused detections in the areas of interest. These images replace the areas of interest with unfocused detections. Fig. 8 shows these replacements with the background given by the TerraSAR-X image. We see that

1) One detection is obtained with the first local GMTI block and one with the second block.
2) These two detections are close to each other.
3) They can be refocused by very similar normalized relative speeds.

With the reference to the criteria for data fusion given in Section IV, the detections are classified to be ground moving target. The local coordinates of the focused moving target (corresponding to the peaks) are $(x_1, y_1) = (390.9, 93.35)$ and $(x_2, y_2) = (343.1, 123.3)$ giving a distance of 56.4 m in the slant range plane. To find the true distance in the ground range, the distance in the slant range should be scaled with the sine of the incident angle (36°). The true distance that the truck had been moving between two measurements is therefore 86.7 m. With the time separation of 10 s between the measurements, the speed of the moving target is 8.67 m/s or about 31.2 km/h that is matched with the speed of the deployed truck. The driving direction can also be estimated to be about 69.78°. This value is matched to the road, in which the truck was moving along. There is a small difference between the normalized relative speeds provided by the first and second local GMTI blocks. It can be the result of slightly different orbits of the SAR systems operating in the monostatic pursuit mode or it can be the small change in speed or direction of the truck. All of them can cause this small difference. The calculation based on (x_1, y_1) and (x_2, y_2) gives the value $\gamma \approx 0.9996$.

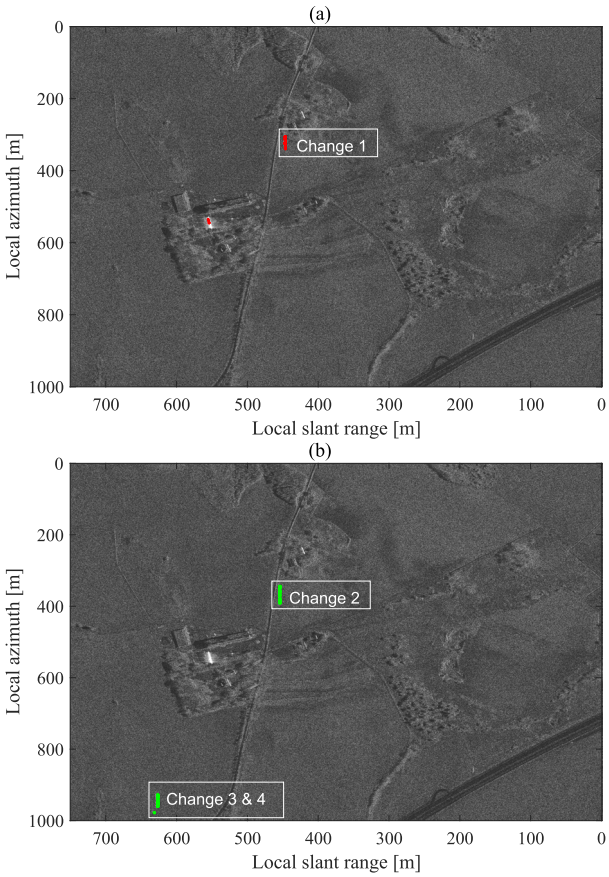

Fig. 9. Change detection results for area of interest marked by dashed-line rectangle in Fig. 4. (a) Reference: TerraSAR-X, surveillance: TanDEM-X. (b) Reference: TanDEM-X, surveillance: TerraSAR-X.

E. Practical Issues

During the measurements, several vehicles were deployed on the SAR scene. We consider here the next area of interest marked by the dash-line rectangle in Fig. 4. The road in the middle of the dashed-line rectangle was a local street where two vehicles (a light military vehicle referring to Target 2 in Table II a moving truck referring to Target 3 in Table II) drove in the same direction (northward) with different speeds. The truck was driven at a low speed initially and then it was accelerated. The light military vehicle driving behind the truck kept a steady speed.

The change detection results provided by the first and second local GMTI blocks are reported in Fig. 9.

There are two positive changes detected by the change detection block. They are marked by the red dots, in which one in the upper middle part of the area of interest with a clear signature of ground moving target (Change 1). The change detection block indicates three negative changes marked with the green dots, in which three are with a clear signature of ground moving target (Changes 2, 3, and 4). These detections can be analyzed as follows.

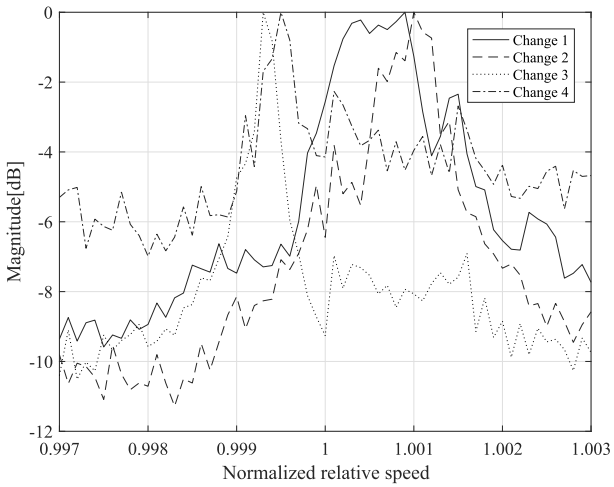

Fig. 10. Graph representing the relationship between normalized relative speed and magnitude (area of interest marked by dashed-line rectangle in Fig. 4).

1) The detections with a clear signature of ground moving target in the upper middle part of the area of interest most likely correspond to a ground moving target.
2) Two remaining detections are the negative changes but not related to any positive change. They are most likely ground moving targets. Due to their movements, they were displaced outside the area of interest.

The local GMTI results with the areas of interest defined with the help of the change detection results are summarized in Fig. 10.

For the first local GMTI block, the peak is found at the hypotheses $\gamma = 1.0009$, at which the detected change is refocused (Change 1). This indicates that the change detected by the change detection block can be a ground moving target with a normalized relative speed of $\gamma \approx 1.0009$. However, there are certain reasons that the magnitudes surrounding the peak are also high. One of them can be the acceleration of the moving truck during the measurements. Another reason can be the interference of the reflections from the moving truck and the light military vehicle, as for several pixels in the images both the targets contribute to the pixel values.

For the second local GMTI block, we retrieve two distinguishable peaks at the hypotheses $\gamma = 0.9993$ and $\gamma = 0.9995$, at which the changes are best refocused (Changes 3 and 4). The results are interpreted as that the two negative changes detected by the change detection block are most likely ground moving targets with a normalized relative speed of $\gamma \approx 0.9993$ and $\gamma \approx 0.9995$. The same problem caused by acceleration and/or signal interference can be observed in the graph representing the relationship between normalized relative speed and magnitude for the remaining detected change (Change 2). Although the peak is found at $\gamma = 1.001$ but the magnitudes surrounding the peak are also high.

The first and second local GMTI blocks provide two detections with similar normalized relative speeds, $\gamma = 1.0009$ and $\gamma = 1.001$, and they are close to each other. Fig. 11 shows the area of interest for change detection (marked by the dashed-line rectangle in Fig. 4) with integrated images of detections. With the reference to the criteria for data fusion given in Section IV, the detections are classified to be ground moving target. The local coordinates of the focused moving target are $(x_1, y_1) = (453.8, 359.9)$ and $(x_2, y_2) = (446.1, 313.8)$. The speed of the moving target is estimated at 4.99 m/s or 17.9 km/h. The driving direction can also be estimated to be about 164.8°. This driving direction is matched to the road on which the military vehicle and the moving truck were moving along. The estimated speed is below the speed of the military vehicle but can be associated with the deployed moving truck with acceleration. The calculation based on (x_1, y_1) and (x_2, y_2) gives the value $\gamma \approx 1.0006$. The value $\gamma = 1.001$ corresponds to another speed of about 25 km/h that is the speed of the military vehicle used in the measurements. The concluding remark is that both the acceleration and the signal interference caused difficulty in detecting moving targets and estimating motion parameters.

Two remaining detected changes are unknown and supposed to be ground moving targets present in the SAR scene. They are close together and have similar normalized relative speeds. To estimate their motion parameters, another area of interest, just below the currently considered area, is selected for the change detection for the GMTI method. However, with currently available information about the estimated γ, different hypotheses can also be given for them. For example, they might be targets moving on the same road at different speeds. They might be moving on different roads. Further investigations on these targets are required before making conclusions about them. However, these investigations will not be covered by this study.

VII. Performance Analysis

In Section VI, the experiment results are based on two areas of interest and three deployed vehicles (Target 1, Target 2, and Target 3). Besides this, there were others ground moving targets that had been deployed in the SAR scene. The list of target deployments is summarized in Table II. Among 11 targets, 7 are detected by the change detection method, whereas 4 are not detected for explainable reasons.

1) Target 4 moved behind the truck and it seems to be partially obscured by the truck.
2) Targets 5 and 6 moved along a road with strong backscattering. It is therefore difficult for the change detection method to detect the changes.
3) Due to the road condition (highway), Target 7 could not keep moving at low speed. The target went beyond the SAR scene.

The detection probability is calculated by the number of employed targets to the number of detected targets. The calculation of detection probability excludes target 5 due to the unwanted situation. Hence, the change detection method gives a detection probability of 70%.

The average error in speed estimation is the average value of the relative errors calculated for each speed estimation. There are totally seven speed estimations corresponding to seven

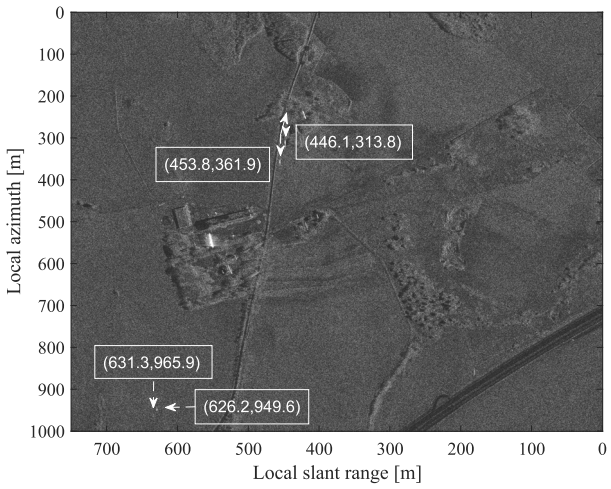

Fig. 11. Area of interest for change detection with integrated images of detections (marked by dashed-line rectangle in Fig. 4).

detected targets. A value of 0.1 is obtained for the average error or in other words 10%.

The average error in direction estimation is calculated using the same principle. There are also totally seven direction estimations corresponding to seven detected targets. The average value of the relative errors calculated for each direction estimation is shown to be 0.03 or 3%.

VIII. Conclusion

In this article, we reviewed some mathematical backgrounds concerning the signature and the displacement of ground moving target in a SAR image. They are the bases of focusing on the target and the local GMTI method. This article also reviewed some SAR change detection methods and one of them was selected for investigating the possibilities to detect ground moving targets using change detection and to combine change detection and GMTI. The SAR change detection method is developed on a new form of likelihood ratio test that avoids unwanted assumptions about target.

A change detection for the GMTI method was proposed for SAR systems operating in the monostatic pursuit mode. The processing scheme of the method is a combination of SAR change detection and SAR GMTI. Two SAR change detection blocks with exchanged roles of reference and surveillance are used to detect possible ground moving targets. They are followed by two local GMTI blocks that help to classify the detected changes. A data fusion block provides the images of detected changes, GMTI results, and the estimated parameters of ground moving targets. In the case where the clutter and noise presented in the data are symmetrically distributed and the clutter and noise model is therefore represented by a symmetrical probability distribution density function, only a single change detection block is required.

Some GMTI results are provided in this article based on the data from the controlled measurements using TerraSAR-X and TanDEM-X conducted in Sweden in 2015. TerraSAR-X and TanDEM-X were operating in the monostatic pursuit mode with the time separation between the measurements of 10 s. In the ground scene, a few moving targets was deployed and two of them was used in this study to test and evaluate the change detection for GMTI method. The GMTI results showed that the method can detect ground moving targets and estimate the parameters of the detected targets.

To further evaluate the change detection for the GMTI method, it is necessary to have an experiment with a large number of targets that will be our future work.

Acknowledgment

The authors would like to acknowledge Airbus Defense and Space for the SAR images provided, and the colleagues at FOI and BTH for helping out during the measurements.

References

[1] R. Linnehan, L. Perlovsky, I. C. Mutz, M. Rangaswamy, and J. Schindler, "Detecting multiple slow-moving targets in SAR images," in *Proc. IEEE Sensor Array Multichannel Signal Process. Workshop*. Barcelona, Spain, Jul. 2004, pp. 643–647.

[2] M. Jahangir and C. P. Moate, "Utilising signal absence in SAR imagery for moving target detection," in *Proc. IET Forum Waveform Diversity Design Commun., Radar Sonar*. London, U.K., Nov. 2006, pp. 41–46.

[3] J. K. Jao, "Theory of synthetic aperture radar imaging of a moving target," *IEEE Trans. Geosci. Remote Sens.*, vol. 39, no. 9, pp. 1984–1992, Sep. 2001.

[4] J. R. Fienup, "Detecting moving targets in SAR imagery by focusing," *IEEE Trans. Aerosp. Electron. Syst.*, vol. 37, no. 3, pp. 749–809, Jul. 2001.

[5] L. M. H. Ulander, M. Lundberg, W. Pierson, and A. Gustavsson, "Change detection for low-frequency SAR ground surveillance," *IEE Proc.-Radar, Sonar Navigat.*, vol. 152, no. 6, pp. 413–420, Dec. 2005.

[6] V. T. Vu, N. R. Gomes, M. I. Pettersson, P. Dammert, and H. Hellsten, "Bivariate gamma distribution for wavelength-resolution SAR change detection," *IEEE Trans. Geosci. Remote Sens.*, vol. 57, no. 1, pp. 473–481, Jan. 2018.

[7] R. Werninghaus and S. Buckreuss, "The TerraSAR-X mission and system design," *IEEE Trans. Geosci. Remote Sens.*, vol. 48, no. 2, pp. 606–614, Feb. 2010.

[8] G. Krieger *et al.*, "TanDEM-X: A satellite formation for high-resolution SAR interferometry," *IEEE Trans. Geosci. Remote Sens.*, vol. 45, no. 11, pp. 3317–3341, Nov. 2007.

[9] P. Lumsdon, M. Schlund, F. V. Poncet, J. Janoth, D. Weihing, and L. Petrat, "An encounter with pursuit monostatic applications of TanDEM-X mission," in *Proc. IEEE IGARSS*. Milan, Italy, Jul. 2015, pp. 3187–3190.

[10] M. I. Pettersson, "Detection of moving targets in wideband SAR," *IEEE Trans. Aerosp. Electron. Syst.*, vol. 40, no. 3, pp. 780–796, Jul. 2004.

[11] V. T. Vu, T. K. Sjögren, and M. I. Pettersson, "Moving target focusing in SAR image with known normalized relative speed," *IEEE Trans. Aerosp. Electron. Syst.*, vol. 53, no. 2, pp. 854–861, Apr. 2017.

[12] C. Cafforio, C. Prati, and F. Rocca, "SAR data focusing using seismic migration techniques," *IEEE Trans. Aerosp. Electron. Syst.*, vol. 27, no. 2, pp. 194–207, Mar. 1991.

[13] M. I. Pettersson, "Optimum relative speed discretisation for detection of moving objects in wide band SAR," *IET Radar, Sonar Navigat.*, vol. 1, no. 3, pp. 213–220, Jun. 2007.

[14] M. Lundberg, L. M. H. Ulander, W. E. Pierson, and A. Gustavsson, "A challenge problem for detection of targets in foliage," *Proc. SPIE*, vol. 6327, pp. 160–171, Apr. 2006.

[15] N. R. Gomes, M. I. Pettersson, V. T. Vu, P. Dammert, and H. Hellsten, "Likelihood ratio test for incoherent wavelength-resolution SAR change detection," in *Proc. CIE Int. Radar Conf.* Guangzhou, China, Oct. 2016, pp. 420–423.

[16] H. Hellsten and R. Machado, "Bayesian change analysis for finding vehicle size targets in VHF foliage penetration SAR data," in *Proc. IEEE Radar Conf.* Johannesburg, South Africa, Oct. 2015, pp. 510–515.

[17] V. T. Vu, M. I. Pettersson, and T. Sjögren, "New forms of likelihood ratio test for SAR change detection," *IEEE Access*, vol. 9, pp. 127906–127916, 2021.

[18] T. Sjögren, V. T. Vu, and M. I. Pettersson, "Experimental result for SAR GMTI using monostatic pursuit mode of TerraSAR-X and TanDEM-X on staring spotlight images," in *Proc. EUSAR*. Hamburg, Germany, Jun. 2016, pp. 207–210.
[19] H. Breit, T. Fritz, U. Balss, M. Lachaise, A. Niedermeier, and M. Vonavka, "TerraSAR-X SAR processing and products," *IEEE Trans. Geosci. Remote Sens.*, vol. 48, no. 2, pp. 727–740, Feb. 2010.
[20] S. Suchandt *et al.*, "Results from an airborne SAR GMTI experiment supporting TerraSAR-X traffic processor development," in *Proc. IEEE IGARSS*. Seoul South Korea, Jul. 2005, pp. 2949–2952.
[21] S. Suchandt, H. Runge, H. Breit, U. Steinbrecher, A. Kotenkov, and U. Balss, "Automatic extraction of traffic flows using TerraSAR-X along-track interferometry," *IEEE Trans. Geosci. Remote Sens.*, vol. 48, no. 2, pp. 807–819, Feb. 2010.
[22] S. Baumgartner, G. Krieger, and K.-H. Bethge, "A large along-track baseline approach for ground moving target indication using TanDEM-X," in *Proc. IEEE IRS*. Cologne, Germany, Sep. 2007, p. 5.
[23] P. Prats-Iraola *et al.*, "High precision SAR focusing of TerraSAR-X experimental staring spotlight data," in *Proc. IEEE IGARSS*. Munic, Germany, Jul. 2012, pp. 3576–3579.

Thomas K. Sjögren (Member, IEEE) received the M.Sc. degree in space engineering from the Luleå University of Technology, Luleå, Sweden, in 2006, the Licentiate degree in applied signal processing, and the Ph.D. degree in applied signal processing from the Blekinge Institute of Technology (BTH), Karlskrona, Sweden, in 2012.

He is currently the Senior Scientist with the Swedish Defense Research Agency (FOI), Linköping, Sweden, working on monostatic, bistatic, and multistatic active and passive radar as well as cognitive radar.

Viet T. Vu (Senior Member, IEEE) received the Ph.D. degree in applied signal processing from the Blekinge Institute of Technology (BTH), Karlskrona, Sweden, in 2011.

Since 2013, he has been with the Department of Mathematics and Natural Science, BTH, where he has been a Post-Doctoral Researcher in radar algorithm development, an Assistant Professor in radar remote sensing, and currently an Associate Professor in system engineering. His major research interests include SAR signal processing, applications of SAR in change detection and SAR GMTI, radio occultation. He has authored or coauthored more than 100 scientific publications.

Mats I. Pettersson (Senior Member, IEEE) received the M.Sc. degree in engineering physics, the Licentiate degree in radio and space science, and the Ph.D. degree in signal processing from the Chalmers University of Technology, Gothenburg, Sweden, 1993, 1995, and 2000, respectively.

For some years, he worked with mobile communication research with Ericsson, Stockholm, and for ten years he was employed with the Swedish Defense Research Agency (FOI), Linköping, Sweden. At FOI he was focusing on ultra wide band low frequency SAR systems. Since 2005, he has been employed with the Blekinge Institute of Technology (BTH), Karlskrona, Sweden, where he is a Full Professor, the Research Director, and a member of the BTH Board of Governors. His work is related to remote sensing where his main interests are SAR inversion and processing, space time adaptive processing (STAP), high resolution SAR change detection, automotive radar and radio occultation.

A. Gustavsson received the M.Sc. degree in applied physics and electrical engineering from Linköping University, Linköping, Sweden, in 1982.

He joined the Swedish Defense Research Agency (FOI), Linköping, in 1982 to work with the implementation of a computer-based SAR processor for microwave systems. He has been involved in the development of airborne low frequency SAR systems since 1990, where his work is in image formation and analysis of data sets registered using monostatic, bistatic, or passive radar modes. He has participated in several field campaigns with airborne and spaceborne SAR sensors, focusing primarily on forestry and foliage penetration problems.